Original

MRI metrics at the epicenter of spinal cord injury are correlated with the stepping process in rhesus monkeys

Jia-Sheng RAO[1], Can ZHAO[2,3], Shu-Sheng BAO[1], Ting FENG[1] and Meng XU[4]

[1]*Beijing Key Laboratory for Biomaterials and Neural Regeneration, Beijing Advanced Innovation Center for Biomedical Engineering, School of Biological Science and Medical Engineering, Beihang University, #37 Xueyuan Road, Haidian District, Beijing, 100191, P.R. China*

[2]*Institute of Rehabilitation Engineering, China Rehabilitation Science Institute, #18 Jiaomen North Road, Fengtai District, Beijing, 100068, P.R. China*

[3]*School of Rehabilitation, Capital Medical University, #10 Xitoutiao, Fengtai District, Beijing, 100069, P.R. China*

[4]*Department of Orthopedics, The First Medical Center of PLA General Hospital, #28 Fuxing Road, Haidian District, Beijing, 100039, P.R. China*

Abstract: Clinical evaluations of long-term outcomes in the early-stage spinal cord injury (SCI) focus on macroscopic motor performance and are limited in their prognostic precision. This study was designed to investigate the sensitivity of the magnetic resonance imaging (MRI) indexes to the data-driven gait process after SCI. Ten adult female rhesus monkeys were subjected to thoracic SCI. Kinematics-based gait examinations were performed at 1 (early stage) and 12 (chronic stage) months post-SCI. The proportion of stepping (PS) and gait stability (GS) were calculated as the outcome measures. MRI metrics, which were derived from structural imaging (spinal cord cross-sectional area, SCA) and diffusion tensor imaging (fractional anisotropy, FA; axial diffusivity, $\lambda_{//}$), were acquired in the early stage and compared with functional outcomes by using correlation analysis and stepwise multivariable linear regression. Residual tissue SCA at the injury epicenter and residual tissue FA/remote normal-like tissue FA were correlated with the early-stage PS and GS. The extent of lesion site $\lambda_{//}$/residual tissue $\lambda_{//}$ in the early stage after SCI was correlated with the chronic-stage GS. The ratios of lesion site $\lambda_{//}$ to residual tissue $\lambda_{//}$ and early-stage GS were predictive of the improvement in the PS at follow-up. Similarly, the ratios of lesion site $\lambda_{//}$ to residual tissue $\lambda_{//}$ and early-stage PS best predicted chronic GS recovery. Our findings demonstrate the predictive power of MRI combined with the early data-driven gait indexes for long-term outcomes. Such an approach may help clinicians to predict functional recovery accurately.

Key words: gait, long-term recovery, magnetic resonance imaging, rhesus monkeys, spinal cord injury

Introduction

Spinal cord injury (SCI), which causes devastating neural damage, can block the transmission of sensory and motor information and thus induces serious dysfunction. Locomotion deficit, one of the common results of a thoracic SCI, severely hampers the mobility, daily life, and social interactions of patients [1–3]. Clinically ef-fective treatments for SCI remain limited [4]. Accurate prediction of long-term functional outcome in the early stage of SCI is one of the goals of SCI diagnosis and can provide reasonable expectations of the degree of recovery to clinicians and patients, as well as a basis for the formulation of rehabilitation protocols [5, 6]. Although research on SCI is widespread, effective prognostic techniques for motor function improvement are lacking [7].

Magnetic resonance imaging (MRI) is a common technique used for diagnosis after SCI. Conventional MRI structural imaging provides useful anatomical information, such as injured segments, injury size, hemorrhage, and edema [8]. Diffusion tensor imaging (DTI), a special MRI technique, can detect the diffusion of water molecules in tissues noninvasively and thus has been adopted to investigate the microstructural integrity of spinal cord axons [9, 10]. Some studies have used conventional structural imaging [11, 12] or combined structural imaging with DTI [13] to identify the image predictors of long-term functional changes. Miyanji *et al.* [11] acquired the three quantitative indexes, maximum spinal cord compression, maximum canal compromise, and lesion length, and six qualitative indexes from MRI of 100 patients with cervical SCI to predict their American Spinal Injury Association (ASIA) motor scores at follow-up. Seif *et al.* [14] established a correlation between the anterior–posterior width of the cervical cord and lower extremity motor (LEM) scores by using a multiparametric MRI protocol. O'Dell *et al.* [15] evaluated MRI and motor functions of 10 patients with SCI and demonstrated a relationship between the midsagittal tissue bridge ratio on structural images and total distance walked in 6 min. A clinical study that combined cervical cord area and voxel-based diffusion indexes demonstrated that atrophy of the ventral horn of the spinal cord is associated with motor output, whereas the integrity of the corticospinal tracts is correlated with spinal cord independence measure (SCIM) scores [16]. In another study, Basso, Beattie, and Bresnahan (BBB) locomotor scores were successfully predicted in spinal cord-contused rats at 3 months post-SCI on the basis of spinal cord area, T2 signal intensity, and DTI indexes at day 1 and 1 month post-SCI [7]. Although these studies have established correlations between some image indicators and motor performances and identified the predictors of long-term outcomes, their predicted targets were macroscopic motor performances or scores that cannot accurately reflect the stepping process of subjects with SCI.

The spatiotemporal characteristics of gait patterns are the output of the locomotion system. Gait characteristics simplify locomotion to interpretable variables to enable the quantitative description of a motor process [17, 18]. The proportion of stepping (PS) is a useful intuitive indicator of gait ability that directly presents the success rate of the stepping process. Gait stability (GS) relies on the precise control of the temporal sequence and burst strength of lower-extremity muscle activity by the central nerve system (CNS) during walking and is an important index that reflects the consistency of the stepping process [19, 20]. GS can be extracted from the degree of vari-

ability in the limb endpoint trajectory during walking and allows for the quantitative reflection of the quality of the stepping process [21, 22].

The aim of this study was to explore whether the MRI metrics obtained from conventional and diffusion imaging after SCI were correlated with the stepping process and predictive of long-term gait status in a rhesus monkey model of partial SCI. We hypothesized that MRI metrics would be good indicators of the PS and GS in the early stage after SCI, whereas early MRI metrics and gait quality could predict the long-term restoration of the PS and GS.

Materials and Methods

Animal preparation

Ten adult female rhesus monkeys (weight, 5–6 kg; age, 4–6 years) were subjected to partial SCI. Female animals were chosen because they are better coordinated and less aggressive than males and are easy to care for after injury. Zoletil 50 (5 mg kg^{-1}) and xylazine hydrochloride (5 mg kg^{-1}) were injected intramuscularly to anesthetize the animals, and sodium pentobarbital (20 mg kg^{-1}, i.v. gtt) was used to maintain anesthesia. The surgery was performed as described previously [23, 24]. Briefly, the right side of the 9th thoracic cord was injured by using microscissors after laminectomy. A piece of tissue with a length of 8–9 mm (rostral–caudal direction) and width of 2–3 mm (left–right direction) was removed under a surgical microscope. After surgery, benzylpenicillin (240 mg) and pentazocine (2 mg kg^{-1}) were intramuscularly administered daily to all animals for approximately 5 days. MRI and kinematics-based gait examinations were performed before and 1 month (early stage) after surgery. The gait examinations were also conducted at 12 months post-SCI (chronic stage) to assess long-term functional recovery (Fig. 1). All experimental procedures were approved by the Biological and Medical Ethics Committee of Beihang University (approval number: BM20180046).

MRI examination

MRI datasets were collected by using Siemens 3T clinical MR equipment (MAGNETOM Skyra, Siemens, Munich, Germany). Animals were positioned in the supine position, and a 32-channel receiver array spine coil was placed at the back of the body [23].

Anatomical images of the spinal cord were acquired by using a proton density (PD)-weighted sequence with the following scan parameters: TR, 3050 ms; TE, 11 ms; matrix, 320 × 320; pixel resolution, 0.6 mm × 0.6 mm; slice thickness, 2 mm; flip angle, 147°; 27 axial slices
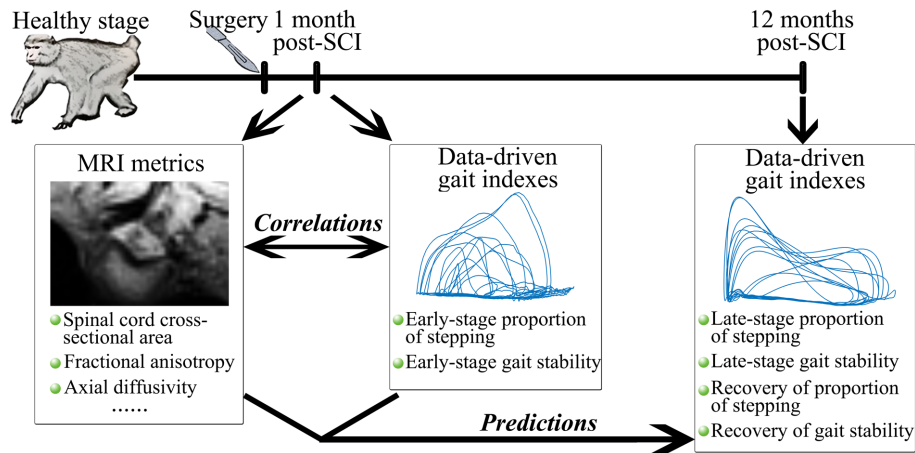
Fig. 1. Conceptual diagram of the experimental design and analysis methods. SCI, spinal cord injury; MRI, magnetic resonance imaging.

without a gap; and coverage of five cord segments (T7–11).

DTI data were acquired at the same center by using a single-shot spin-echo echo planar imaging (EPI) sequence with the following scan parameters: TR, 4500 ms; TE, 104 ms; matrix, 128×128; pixel resolution, 1.5 mm $\times$ 1.5 mm; slice thickness, 2 mm; b, 0 and 1,000 s/mm^2; repeat time, 5; 12 noncollinear gradient directions; and 25 diffusion-weighted axial slices without a gap. Parallel acquisition was used with an acceleration factor of 3 to limit the extent of susceptibility artifacts. A twice-refocused pulse sequence was used to minimize eddy current effects [25, 26]. Saturation bands were set on the chest and abdomen to reduce physiological motion artifacts. The entire scanning time was approximately 14 min.

Gait test

The stepping process of the right (ipsilateral to the injury) hindlimbs of the animals was collected by using a Vicon system (Vicon 8, Oxford Metrics Limited Co., Yamton, UK). A reflective marker was fixed on the second metatarsophalangeal joint, and its spatial location was recorded through multiple cameras in real time (recording frequency: 100 Hz). The animals were allowed to walk on a treadmill bipedally with their upper body restrained (speed: 0.2 m s^{-1}), and successive stepping (>10 steps) data were captured for subsequent analysis [26–29].

Data analysis

A slice centered at the injury epicenter (including the lesion site and residual tissue) and two slices 2 cm from the damaged area (defined as remote normal-like tissue) were used for MRI analysis. Regions of interest (ROIs)

were selected from the axial PD-weighted images. The lesion site, residual tissues, and remote normal-like tissues were manually extracted in accordance with the previously reported signal–intensity–variation (SIV) method [25]. In brief, SIV was calculated as SIV = (LSI − NSI) / LSI, where LSI is the averaged signal intensity within the ROI of the lesion site, and NSI is the averaged signal intensity within the residual or remote normal-like tissues. The PD-weighted SIVs were obtained by comparing the lesion site with the residual tissue (44.3% ± 1.1%) and the lesion site with the remote normal-like tissue (55.5% ± 1.6%). The thresholds of SIV between the lesion site and residual tissue (SIV ≥ 30%) and the lesion site and remote normal-like tissue (SIV ≥ 50%) were then selected as the standards for classifying borderline pixels in the residual and remote normal-like tissues to avoid partial volume effects with the lesion site [25]. The spinal cord cross-sectional areas (SCAs) of the lesion site, residual tissue, and remote normal-like tissue were obtained from the above ROIs.

DTI datasets were processed and analyzed using MedINRIA (http://www-sop.inria.fr/asclepios/software/MedINRIA). The detailed methods were reported previously [23, 25, 26]. For eddy current distortion, five b0 images in EPI datasets were averaged. All diffusion-weighted images were aligned with the averaged b0 image through line affine transformation to correct the mismatch induced by eddy current distortion between b0 and diffusion-weighted images [23]. For geometric distortion, the averaged b0 image was first registered to PD volumes using the diffeomorphic demons registration algorithm to obtain a nonrigid displacement field. Then, the deformation vector field was extracted and applied to all EPI datasets to correct for geometric distortion [23, 30].

The corrected EPI datasets were used to calculate DTI indexes. The ROIs of the lesion site, residual tissue, and remote normal-like tissue were determined on the PD-weighted images. Given that distinguishing gray matter from white matter in the injury epicenter is difficult, gray and white matters were drawn onto the ROI [25]. Three eigenvectors (v_1, v_2, v_3) and the corresponding eigenvalues (λ_1, λ_2, λ_3) of the diffusion tensor matrix were extracted from the above ROIs on a voxel-to-voxel basis [10, 23]. Fractional anisotropy (FA), apparent diffusion coefficient (ADC), axial diffusivity ($\lambda_{//} = \lambda_1$, parallel to the axonal pathways), and radial diffusivity ($\lambda_{\perp} = [\lambda_2 + \lambda_3]/2$, perpendicular to the axonal pathways) values at the lesion site, residual tissue, and remote normal-like tissue were then acquired [8]. The values of the DTI indexes at the lesion site of each animal were divided by their own residual tissue values to decrease the effect of individual variability and by their own remote normal-like tissue values (formulas are given in Fig. 2). The possible correlations among DTI indexes were detected by using Pearson correlation tests. Only noncollinear variables (FA and $\lambda_{//}$) were retained for subsequent analysis (Fig. 2).

The gait datasets were processed and calculated by using custom Matlab-based (MathWorks, Natick, MA, USA) software. The gait cycle was first divided automatically [31]. Then, the step height, stride length, direction and acceleration of the limb endpoint velocity at swing onset, and path length of the limb endpoint trajectory of each gait cycle were computed [28]. The PS and GS were set to decrease the effect of individual variability and to reflect gait performance comprehensively. The PS was defined as the ratio of successful gait cycles (step height >10% of its normal value) per total gait cycle in each animal at each time point (100% indicates totally successful stepping at a time point, and 0% indi-

cates totally dragging at a time point). For GS, each gait parameter relative to its average value for all gait cycles was first computed as the variability. The consistency of each gait parameter was then obtained with the logarithm of the variability. GS was defined as the mean value of the consistency of all gait parameters at each time point for each animal, and its value ranged from 0 (the limb endpoint trajectory was completely different) to 1 (the limb endpoint trajectory was the same). The GS value of the dragged gait cycle was set to 0.

Finally, we obtained nine MRI and gait variables in the early stage of SCI: residual tissue SCA, lesion site SCA/residual tissue SCA, residual tissue SCA/remote normal-like tissue SCA, lesion site FA/residual tissue FA, residual tissue FA/remote normal-like tissue FA, lesion site $\lambda_{//}$/residual tissue $\lambda_{//}$, residual tissue $\lambda_{//}$/remote normal-like tissue $\lambda_{//}$, PS_{early}, and GS_{early}. Four gait indexes in the chronic stage of SCI were also obtained: $PS_{chronic}$, $GS_{chronic}$, ΔPS ($\Delta PS = PS_{chronic} - PS_{early}$), and ΔGS ($\Delta GS = GS_{chronic} - GS_{early}$).

Statistics

Statistical analysis was conducted by using IBM SPSS Statistics 20.0 (IBM Corp, Armonk, NY, USA). The paired t-test was used to detect the changes in MRI and gait metrics between pre- and post-SCI time points. Bonferroni correction was applied for multiple comparisons. Pearson (normality) or Spearman (non-normality) correlation was executed to explore the relationship between MRI metrics and gait performance. The nonparametric Kolmogorov–Smirnov test was used to examine the normality of MRI and gait metrics. All MRI variables at 1 month post-SCI were included for the prediction of PS_{early} and GS_{early}. For the prediction of long-term stepping status, MRI and gait metrics at 1 month post-SCI were analyzed. Stepwise multivariable linear regression
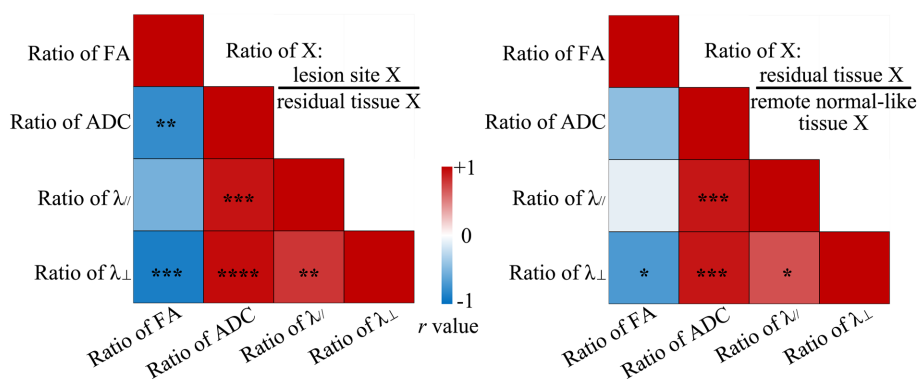

Fig. 2. Correlations among DTI indexes at 1 month post-SCI. The bar indicates the correlation coefficient value. FA, fractional anisotropy; ADC, apparent diffusion coefficient; $\lambda_{//}$, axial diffusivity (parallel to the axonal pathways); $\lambda_{\perp}$, radial diffusivity (perpendicular to the axonal pathways). *$P<0.05$. **$P<0.01$. ***$P<0.001$. ****$P<0.0001$.

was utilized to identify the models that included only significant variables and the highest R^2 regression [32]. The squared partial correlation (Pr^2) between each significant variable and gait performance was calculated to display the proportion of variability in the stepping process that could be explained by each independent variable after the effects of other variables were removed. Data are reported as the mean ± SD. The significance level was set at $P<0.05$.

Results

SCI alters MRI and gait variables

All monkeys were subjected to SCI and subsequent MRI and kinematic assessments. The structure of the normal spinal cord was intact, and the gray and white matters were clearly distinguishable (Fig. 3A). After injury, the spinal cord structure was damaged, and the spinal cord morphology was obviously altered. Reductions in visible tissue areas in the injured site reflected injury-induced atrophy (Fig. 3A). Longitudinal comparisons showed that the residual tissue SCA was significantly smaller than its normal states, and its ratio with the remote normal-like tissue SCA was also reduced (Fig. 3B). At 1 month post-SCI, residual tissue FA/remote normal-like tissue FA exhibited a clear decrease, whereas residual tissue $\lambda_{//}$/remote normal-like tissue $\lambda_{//}$ remained stable (Fig. 3B). Animals could complete stepping in the normal state (PS: 100%), and the stability of

the hindlimb endpoint trajectory was 0.830 ± 0.032. In the early stage after SCI, the PS (52.971% ± 32.409%) and GS (0.366 ± 0.209) of the hindlimb ipsilateral to the injury exhibited pronounced deterioration (PS, $P_{corrected}$=0.004; GS, $P_{corrected}$=0.000). After 12 months, the stepping ability of the animals displayed significant improvement (PS, 93.571% ± 15.954%, $P_{corrected}$=0.009 for 12 months (mo.) vs. 1 mo., $P_{corrected}$=0.704 for 12 mo. vs. normal; GS: 0.724 ± 0.127, $P_{corrected}$=0.003 for 12 mo. vs. 1 mo., $P_{corrected}$=0.104 for 12 mo. vs. normal; Fig. 3C).

MRI metrics reflect early-stage gait ability

The relationships of MRI metrics with the PS and GS at the same time point in the early stage after SCI were analyzed (Table 1). The ratio of residual tissue SCA to remote normal-like tissue SCA exhibited the strongest correlation with the PS (r=0.785, P=0.007) and GS (r=0.795, P=0.006), whereas the variables extracted from DTI showed no obvious correlation with either the PS or GS (P>0.05).

By using stepwise multivariable linear regression, we analyzed all seven predefined variables (MRI metrics) as indicators of gait ability (PS and GS). The best model for reflecting early-stage PS (adjusted R^2=0.874, P=0.000) and GS (adjusted R^2=0.866, P=0.000) included residual tissue SCA and residual tissue FA/remote normal-like tissue FA (Table 2).
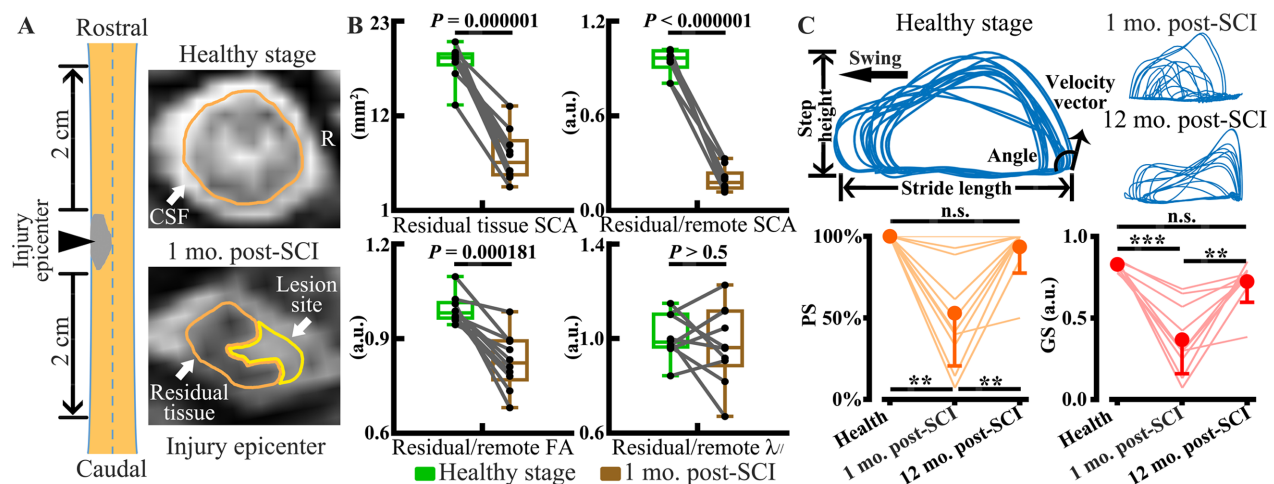

Fig. 3. SCI alters the spinal cord architecture and gait performances of animals. (A) Representative axial PD-weighted structural images displaying the alterations in spinal cord morphology at the injury epicenter. (B) MRI metrics significantly changed after injury. Box plots presenting the median and 25th and 75th percentiles; whiskers indicate the minimum and maximum values. Dots represent individual values. (C) Typical results showing the successive trajectories (n>10 steps) of the hindlimb endpoint ipsilateral to the injury in the healthy state and at 1 and 12 months post-SCI. The thin arrow indicates the direction of the limb endpoint velocity at swing onset. Longitudinal changes in the PS and GS are shown. Large circles show the average per time point. Data are means ± SD. Lines represent individual variations. CSF, cerebrospinal fluid; SCA, spinal cord cross-sectional area; FA, fractional anisotropy; $\lambda_{//}$, axial diffusivity (parallel to the axonal pathways); PS, proportion of stepping; GS, gait stability; mo., months. *$P<0.05$. **$P<0.01$. ***$P<0.001$.

Table 1. Correlations between the MRI and gait metrics at 1 month post-SCI

		Residual tissue SCA	Lesion site SCA/residual tissue SCA	Residual tissue SCA/remote tissue SCA	Lesion site FA/residual tissue FA	Residual tissue FA/remote tissue FA	Lesion site $\lambda_{//}$/residual tissue $\lambda_{//}$	Residual tissue $\lambda_{//}$/remote tissue $\lambda_{//}$
PS	*r*	0.764*	−0.599	0.785**	−0.117	0.524	−0.158	−0.242
	P	0.01	0.067	0.007	0.747	0.12	0.662	0.5
GS	*r*	0.766**	−0.59	0.795**	−0.196	0.515	−0.121	−0.178
	P	0.01	0.073	0.006	0.587	0.127	0.74	0.623

MRI, magnetic resonance imaging; SCI, spinal cord injury; PS, proportion of stepping; GS, gait stability; SCA, spinal cord cross-sectional area; FA, fractional anisotropy; $\lambda_{//}$, axial diffusivity (parallel to the axonal pathways). *$P<0.05$. **$P<0.01$.

Table 2. Multivariable regression analysis of MRI metrics as indicators of the stepping process at 1 month after injury

MRI parameters	PS				GS			
	Standardized coefficient β	*t* value	*P* value	Pr^2 value	Standardized coefficient β	*t* value	*P* value	Pr^2 value
Residual tissue SCA	0.793	6.686	0.00028	0.865	0.795	6.518	0.00033	0.859
Residual tissue FA / remote normal-like tissue FA	0.565	4.765	0.00205	0.764	0.557	4.563	0.00259	0.748

MRI, magnetic resonance imaging; PS, proportion of stepping; GS, gait stability; SCA, spinal cord cross-sectional area; FA, fractional anisotropy; Pr^2, squared partial correlation.
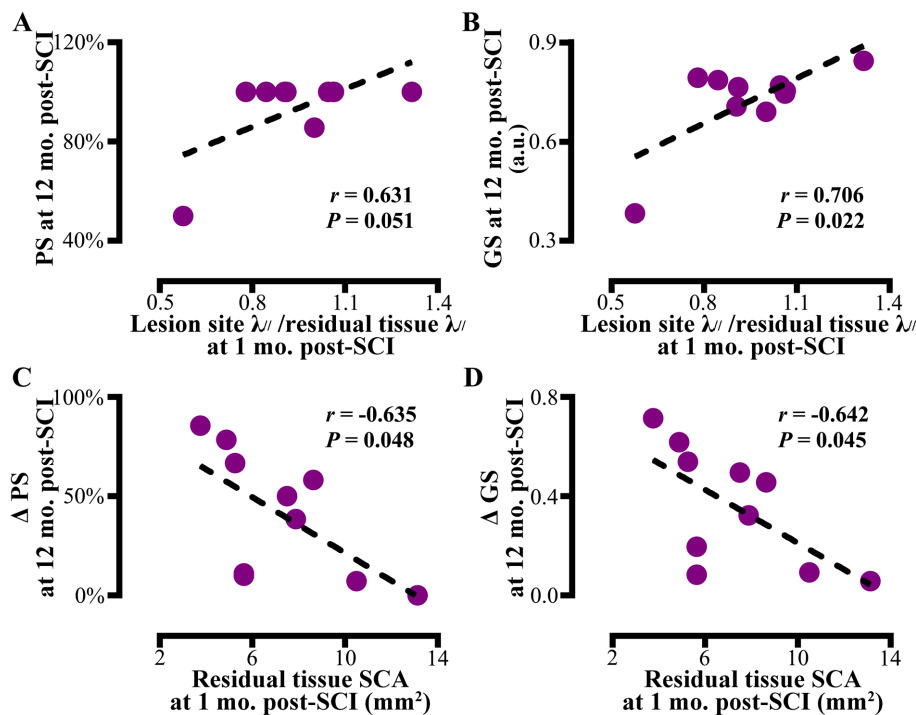

Fig. 4. Relationships between PS (A) and GS (B) at 12 months post-SCI and lesion site $\lambda_{//}$/residual tissue $\lambda_{//}$ at 1 month post-SCI and between ΔPS (C) and ΔGS (D) in the chronic stage and residual tissue SCA in the early stage. PS, proportion of stepping; GS, gait stability; $\lambda_{//}$, axial diffusivity (parallel to the axonal pathways); SCA, spinal cord cross-sectional area; *r*, correlation coefficient; mo., months.

MRI metrics are correlated with chronic-stage gait ability

MRI metrics and gait indexes in the early stage were also evaluated in terms of their relationship with the long-term stepping process. No marked correlation was observed between the PS in the chronic stage and MRI metrics at 1 month post-SCI ($P>0.05$). However, a close but not significant correlation between PS in the chronic stage and lesion site $\lambda_{//}$/residual tissue $\lambda_{//}$ in the early stage was observed ($r=0.631$, $P=0.051 > 0.05$; Fig. 4A). A significant relationship was found between GS in the chronic stage and lesion site $\lambda_{//}$/residual tissue $\lambda_{//}$ in the

Table 3. Multivariable regression analysis of early-stage MRI and gait variables as predictors of long-term gait improvement

MRI/gait variables	ΔPS at 12 months post-SCI				MRI/gait variables	ΔGS at 12 months post-SCI			
	Standardized coefficient β	t value	P value	Pr^2 value		Standardized coefficient β	t value	P value	Pr^2 value
Lesion site $\lambda_{//}$ / residual tissue $\lambda_{//}$	0.376	3.416	0.0112	0.227	Lesion site $\lambda_{//}$ / residual tissue $\lambda_{//}$	0.357	2.145	0.069117	0.397
GS_{early}	−0.836	−7.602	0.00013	0.777	PS_{early}	−0.772	−4.637	0.002378	0.754

MRI, magnetic resonance imaging; ΔPS, change in proportion of stepping; ΔGS, change in gait stability; $\lambda_{//}$, axial diffusivity (parallel to the axonal pathways); GS_{early}, proportion of stepping in the early stage; PS_{early}, gait stability in the early stage; Pr^2, squared partial correlation.

early stage (r=0.706, P=0.022; Fig. 4B). Gait indexes in the chronic stage showed no relationship with PS_{early} and GS_{early} (P>0.05). In addition, ΔPS (r=−0.635, P=0.048) and ΔGS (r=−0.642, P=0.045) were correlated with residual tissue SCA at 1 month post-SCI (Figs. 4C, D).

By using stepwise multivariable linear regression, we analyzed all predefined early-stage variables (MRI and gait metrics) as predictors of long-term ΔPS and ΔGS. The best model for predicting the long-term ΔPS included GS_{early} and lesion site $\lambda_{//}$/residual tissue $\lambda_{//}$ at 1 month post-SCI (adjusted R^2=0.893, P=0.000; Table 3). The best model for predicting the long-term ΔGS included PS_{early} and lesion site $\lambda_{//}$/residual tissue $\lambda_{//}$ at 1 month post-SCI (adjusted R^2=0.757, P=0.003; Table 3).

Discussion

In this study, we detected the changes in MRI metrics in the early stage of thoracic SCI, as well as the changes in the long-term stepping process after thoracic SCI, and established the associations of MRI metrics with gait performances in the early and chronic stages. By using stepwise multivariable linear regression, we determined that the extents of residual tissue SCA and residual tissue FA/remote normal-like tissue FA were the key indicators of early-stage stepping ability after injury. However, only the extent of lesion site $\lambda_{//}$/residual tissue $\lambda_{//}$ at 1 month post-SCI was correlated with chronic-stage GS. For long-term gait improvements, only the extents of lesion site $\lambda_{//}$/residual tissue $\lambda_{//}$ and early-stage stepping ability showed significant correlations in multivariable regression analysis.

SCI disrupts the integrity of the spinal cord architecture. In the absence of an effective clinical regenerative technique, the residual tissue in the injury epicenter, which is the physiological basis for restoring function, is important for connecting the supraspinal center and structures below the injury level [33, 34]. Some studies have applied MRI data from acute SCI (1–3 days after injury) for predicting functional recovery [11, 13]. However, MRI signal changes are not specific to the underlying pathophysiology [35] and can reflect various pro-cesses, such as hemorrhage, cytotoxic edema, and cord swelling [36–38]. Since a severe pathophysiological response occurs in the acute stage after injury, the signal of residual tissue tends to be masked by those of hemorrhage and edema. For this reason, the evaluation of the signal can change considerably over time and is highly variable across patients [37], making accurate assessment of the residual tissue unfavorable. Considering the stability of MRI image quality, one month after SCI was set as the time point for MRI scans. Two clinical studies [15, 39] have shown that small residual tissues could be measured with the gradually vanishing of hemorrhage and edema at 1 month post-SCI. We retained the noncollinear FA and $\lambda_{//}$ variables to evaluate the status of spinal cord tissues but eliminated the ADC variable because it is less sensitive to the effects of SCI than other variables [8, 40]. Our findings showed a pronounced reduction in the ratio of residual tissue FA to remote normal-like tissue FA. Such a reduction was indicative of the loss of the diffusion anisotropy of water molecules in the residual tissue. However, the diffusivity parallel to the axonal pathways remained stable after injury. This showed that the axonal pathways in the residual tissue were preserved [41, 42] but underwent demyelination [43].

A previous research explored the gait performance of rhesus monkeys with C7 cord hemitransection and found a significant improvement in hindlimb dragging and an obvious recovery in the consistency of the amplitude of the hip, knee, ankle, and toe joint movements at 6 months after injury [44]. Another study on mice with thoracic cord hemitransection also reported an improvement in the length of the hindlimb gait and the myoelectric activity amplitude of the vastus lateralis (extensor) and tibialis anterior (flexor) during stepping at 3 months post-SCI [45]. The results of the present study are similar to those of previous reports in that the stepping ability of the animals was impaired in the early phase but gradually improved. This result indicated great potential for plasticity after partial SCI.

Numerous factors affect motor functions after SCI, and these factors have been analyzed in many studies

[46–48]. Despite variations in estimates across studies, the generalized predictive outcome of ambulation and other functional activities largely depends on the severity of the injury and the scores of the related functional assessments [49, 50]. The score data used in clinical and animal SCI prediction studies are usually derived from qualitative and/or semiquantitative scales, such as SCIM scores, functional independence measure scores, ASIA impairment scale (AIS) grades, International Standards for Neurological Classification of Spinal Cord Injury classifications, spinal cord ability ruler scores, BBB scores, and Basso mouse scale scores. Although widely used, these neurological tools struggle to reflect a high degree of variability in outcomes, as well as to differentiate differences in motor processes finely, thus complicating the prediction of long-term functional changes in SCI [7, 51]. In this study, the advantages of using kinematics-based gait analysis for predictive analysis over functional assessments were (i) the availability of an objective, data-driven description of gait performances that thus avoids the subjective influence of scale scores [51, 52] and (ii) the ability to describe each stepping process and accurately distinguish gait differences, which facilitates the determination of highly variable functional outcomes.

In the early stage after SCI, the PS and GS were correlated with residual tissues in the injury epicenter; this correlation indicated the importance of residual tissue for maintaining locomotion [33, 34]. Although the ratio of residual tissue SCA to remote normal-like tissue SCA has a significant correlation with the PS and GS, its power as an indicator is weaker than that of multivariate association given that conventional structural images cannot fully reflect the status of projection pathways [35]. By contrast, the areas of residual tissue, along with the ratio of residual tissue FA to remote normal-like tissue FA, have shown strong power to reflect the PS and GS, thus suggesting that the ability to control gait relies not only on the amount of residual tissue (areas) but also the quality (microstructural integrity) of residual tissue at the injury epicenter.

Notably, no significant relationship was observed between the early- and chronic-stage gait performances in this study. In contrast to our work, a previous study established a prediction model for mobility performance in the SCIM at 1-year follow-up by using the age of the patient with SCI, the motor scores of the quadriceps femoris (L3) and gastrocsoleus (S1) muscles, and the light touch sensation of dermatomes L3 and S1 [53]. A subsequent multicenter prospective study simplified these predictors to three: age, motor score of L3, and light touch score of S1 [54]. Another clinical study on

incomplete SCI combined LEM scores with pinprick scores or age-predicted walking ability in patients at 6 months post-SCI [55]. A recent study successfully predicted the recovery of independent function by using the AIS grade and LEM scores [56] but discovered that the strongest outcome predictor (LEM score) was different from that (sensory score for light touch) found in a previous study [57]. The inconsistency of the present study with previous studies may be attributed to two reasons: (i) The exclusion of sensory-related variables from our metrics may have affected our ability to reveal the connection between early and chronic gait performance. Previous studies have demonstrated that the preservation of sensory function is fundamental to the maintenance of walking ability [58, 59]. A survey by Scivoletto *et al.* [48] also showed that >60% of patients with light touch and pinprick preservation recovered ambulation at 1 year postinjury. (ii) Binary classification (walk or not walk) was the most commonly used outcome to reflect exercise capacity in previous studies [53–55, 57]. In this study, however, PS and GS were set as outcomes to reveal the improvement in the stepping process and to reflect the alterations in gait performance accurately.

According to their definitions, PS and GS reflect different aspects of gait performance. PS mainly demonstrates whether the animal achieves the swing phase, whereas GS additionally estimates the stability and consistency of the stepping process. In primates, highly stable and consistent gait cycles (GS) require more precise supraspinal control than achieving swing (PS) [27, 60, 61]. The integrity of cortical projection pathways determines the degree of supraspinal control after SCI. Consistently, a positive relationship was only found between the ratio of lesion site $\lambda_{//}$ to residual tissue $\lambda_{//}$ and GS. This result suggested that good axonal integrity in the injury zone has the potential to improve the homogeneity of gait cycles.

Although long-term ΔPS and ΔGS were associated with residual tissue SCA in the early stage of SCI, the multivariable linear regression analysis included the ratio of lesion site $\lambda_{//}$ to residual tissue $\lambda_{//}$ and early-stage gait performances as the key predictors. The standardized coefficient β of the lesion site $\lambda_{//}$/residual tissue $\lambda_{//}$ indicated positive correlations between axonal integrity at the lesion site and ΔPS or ΔGS. However, moderate changes in long-term ΔPS and ΔGS in animals with initial high GS and PS may be due to a ceiling effect [51].

This study has several limitations. First, accurate prediction results are more valuable when they are obtained early in the clinic. Our MRI datasets for the early stage, however, were acquired at 1 month post-SCI to match kinematics-based gait examinations. In general, progres-

sion of SCI pathophysiology is similar between species [62]. However, Smith *et al.* [63] reported that lower mammals have shorter shock phases after SCI than humans. According to this tendency, we believe that 1 month post-SCI in rhesus monkeys corresponds to a similar or even later time point in humans. Although some reports have suggested that MRI at 2–3 weeks after injury may be beneficial in assessing correlations [11, 64], prediction in the acute phase is highly useful for treatment. Second, no sensory-related variables were included in this study. Sensory-related variables should be included in further studies because the status of sensory functions after injury is important for assessing the potential for recovery. Finally, as this was a preliminary study, only the injury site of a partial transection model was investigated; this approach limited the ability of the study to reveal potential relationships between changes beyond the damaged zone and functional improvement [65, 66] and precluded it from mimicking the complexity of clinical injury types. The correlations between gait performance and widespread alterations in the CNS under various SCI types and degrees need to be explored. Furthermore, the existing evidence suggests that older SCI patients experience a similar degree of sensorimotor recovery as younger ones but with great functional deficits [67]. Since only young adult monkeys (4–6 years old) were used in this study, the applicability of the findings to older subjects still needs to be further evaluated.

Conclusions

Our study showed that MRI and kinematics-based gait examinations in the early stage after SCI were useful tools in predicting the long-term recovery of the stepping process in a primate model of partial thoracic transection. The area and microstructural integrity of residual tissue at the injury epicenter were found to be better determinants of early-stage gait performance than the ratio of residual tissue areas to remote normal-like tissues. Although diffusion anisotropy is commonly used in diagnostic studies, $\lambda_{//}$ (diffusivity parallel to the axonal pathway) may be more important than other indexes in assessing potential functional recovery because it is correlated with chronic GS and is a predictor of the prognosis of gait improvements. The increased sensitivity of the MRI and gait metrics applied in this work may allow for the quantitative evaluation of data-driven gait performances. Such an evaluation may have the potential to provide precise expectations for functional recovery in clinical studies.

References

1. Rossignol S, Schwab M, Schwartz M, Fehlings MG. Spinal cord injury: time to move? J Neurosci. 2007; 27: 11782–11792. [Medline] [CrossRef]
2. Harkema S, Gerasimenko Y, Hodes J, Burdick J, Angeli C, Chen Y, et al. Effect of epidural stimulation of the lumbosacral spinal cord on voluntary movement, standing, and assisted stepping after motor complete paraplegia: a case study. Lancet. 2011; 377: 1938–1947. [Medline] [CrossRef]
3. Xiao Z, Tang F, Tang J, Yang H, Zhao Y, Chen B, et al. One-year clinical study of NeuroRegen scaffold implantation following scar resection in complete chronic spinal cord injury patients. Sci China Life Sci. 2016; 59: 647–655. [Medline] [CrossRef]
4. Alizadeh A, Dyck SM, Karimi-Abdolrezaee S. Traumatic spinal cord injury: an overview of pathophysiology, models and acute injury mechanisms. Front Neurol. 2019; 10: 282. [Medline] [CrossRef]
5. Sturt R, Hill B, Holland A, New PW, Bevans C. Validation of a clinical prediction rule for ambulation outcome after non-traumatic spinal cord injury. Spinal Cord. 2020; 58: 609–615. [Medline] [CrossRef]
6. Ditunno JF Jr. The John Stanley Coulter Lecture. Predicting recovery after spinal cord injury: a rehabilitation imperative. Arch Phys Med Rehabil. 1999; 80: 361–364. [Medline] [CrossRef]
7. Wilkins N, Skinner NP, Motovylyak A, Schmit BD, Kurpad S, Budde MD. Evolution of magnetic resonance imaging as predictors and correlates of functional outcome after spinal cord contusion injury in the rat. J Neurotrauma. 2020; 37: 889–898. [Medline] [CrossRef]
8. Zhao C, Rao JS, Pei XJ, Lei JF, Wang ZJ, Zhao W, et al. Diffusion tensor imaging of spinal cord parenchyma lesion in rat with chronic spinal cord injury. Magn Reson Imaging. 2018; 47: 25–32. [Medline] [CrossRef]
9. Bao SS, Zhao C, Bao XX, Rao JS. Effect of b value on imaging quality for diffusion tensor imaging of the spinal cord at ultrahigh field strength. BioMed Res Int. 2021; 2021: 4836804. [Medline] [CrossRef]
10. Zhao C, Rao JS, Pei XJ, Lei JF, Wang ZJ, Yang ZY, et al. Longitudinal study on diffusion tensor imaging and diffusion tensor tractography following spinal cord contusion injury in rats. Neuroradiology. 2016; 58: 607–614. [Medline] [CrossRef]
11. Miyanji F, Furlan JC, Aarabi B, Arnold PM, Fehlings MG. Acute cervical traumatic spinal cord injury: MR imaging findings correlated with neurologic outcome--prospective study with 100 consecutive patients. Radiology. 2007; 243: 820–827. [Medline] [CrossRef]
12. Smith AC, Albin SR, O'Dell DR, Berliner JC, Dungan D, Sevigny M, et al. Axial MRI biomarkers of spinal cord damage

to predict future walking and motor function: a retrospective study. Spinal Cord. 2021; 59: 693–699. [Medline] [CrossRef]

13. Kim JH, Song SK, Burke DA, Magnuson DS. Comprehensive locomotor outcomes correlate to hyperacute diffusion tensor measures after spinal cord injury in the adult rat. Exp Neurol. 2012; 235: 188–196. [Medline] [CrossRef]

14. Seif M, Curt A, Thompson AJ, Grabher P, Weiskopf N, Freund P. Quantitative MRI of rostral spinal cord and brain regions is predictive of functional recovery in acute spinal cord injury. Neuroimage Clin. 2018; 20: 556–563. [Medline] [CrossRef]

15. O'Dell DR, Weber KA, Berliner JC, Elliott JM, Connor JR, Cummins DP, et al. Midsagittal tissue bridges are associated with walking ability in incomplete spinal cord injury: A magnetic resonance imaging case series. J Spinal Cord Med. 2020; 43: 268–271. [Medline] [CrossRef]

16. Huber E, David G, Thompson AJ, Weiskopf N, Mohammadi S, Freund P. Dorsal and ventral horn atrophy is associated with clinical outcome after spinal cord injury. Neurology. 2018; 90: e1510–e1522. [Medline] [CrossRef]

17. Wei RH, Song W, Zhao C, Zhao W, Li LF, Ji R, et al. Influence of walking speed on gait parameters of bipedal locomotion in rhesus monkeys. J Med Primatol. 2016; 45: 304–311. [Medline] [CrossRef]

18. Nauwelaerts S, Aerts P, D'Août KD. Speed modulation in swimming frogs. J Mot Behav. 2001; 33: 265–272. [Medline] [CrossRef]

19. Fouad K, Ng C, Basso DM. Behavioral testing in animal models of spinal cord injury. Exp Neurol. 2020; 333: 113410. [Medline] [CrossRef]

20. Jordan K, Challis JH, Newell KM. Speed influences on the scaling behavior of gait cycle fluctuations during treadmill running. Hum Mov Sci. 2007; 26: 87–102. [Medline] [CrossRef]

21. Capogrosso M, Milekovic T, Borton D, Wagner F, Moraud EM, Mignardot JB, et al. A brain-spine interface alleviating gait deficits after spinal cord injury in primates. Nature. 2016; 539: 284–288. [Medline] [CrossRef]

22. Wagner FB, Mignardot JB, Le Goff-Mignardot CG, Demesmaeker R, Komi S, Capogrosso M, et al. Targeted neurotechnology restores walking in humans with spinal cord injury. Nature. 2018; 563: 65–71. [Medline] [CrossRef]

23. Rao JS, Liu Z, Zhao C, Wei RH, Liu RX, Zhao W, et al. Image correction for diffusion tensor imaging of Rhesus monkey thoracic spinal cord. J Med Primatol. 2019; 48: 320–328. [Medline] [CrossRef]

24. Rao JS, Zhao C, Zhang A, Duan H, Hao P, Wei RH, et al. NT3-chitosan enables de novo regeneration and functional recovery in monkeys after spinal cord injury. Proc Natl Acad Sci USA. 2018; 115: E5595–E5604. [Medline] [CrossRef]

25. Rao JS, Zhao C, Yang ZY, Li SY, Jiang T, Fan YB, et al. Diffusion tensor tractography of residual fibers in traumatic spinal cord injury: a pilot study. J Neuroradiol. 2013; 40: 181–186. [Medline] [CrossRef]

26. Zhao C, Song W, Rao JS, Zhao W, Wei RH, Zhou X, et al. Combination of kinematic analyses and diffusion tensor tractography to evaluate the residual motor functions in spinal cord-hemisected monkeys. J Med Primatol. 2017; 46: 239–247. [Medline] [CrossRef]

27. Rao JS, Liu Z, Zhao C, Wei RH, Zhao W, Yang ZY, et al. Longitudinal evaluation of functional connectivity variation in the monkey sensorimotor network induced by spinal cord injury. Acta Physiol (Oxf). 2016; 217: 164–173. [Medline] [CrossRef]

28. Wei RH, Zhao C, Rao JS, Zhao W, Zhou X, Tian PY, et al. The kinematic recovery process of rhesus monkeys after spinal cord injury. Exp Anim. 2018; 67: 431–440. [Medline] [CrossRef]

29. Wei RH, Zhao C, Rao JS, Zhao W, Wei YQ, Zhou X, et al. Neuromuscular control pattern in rhesus monkeys during bipedal walking. Exp Anim. 2019; 68: 341–349. [Medline]

30. Cohen-Adad J, Benali H, Hoge RD, Rossignol S. In vivo DTI of the healthy and injured cat spinal cord at high spatial and angular resolution. Neuroimage. 2008; 40: 685–697. [Medline] [CrossRef]

31. Zhao W, Song W, Rao JS, Wei RH, Li LF, Ji R, et al. Gait division of healthy and spinal cord-injured rhesus monkeys by one-dimensional toe signals. J Mech Med Biol. 2018; 18: 1850017. [CrossRef]

32. Tabachnick BG, Fidell LS. Using multivariate statistics, 6th ed. New Jersey: Pearson Education, 2012.

33. Ramer LM, Ramer MS, Bradbury EJ. Restoring function after spinal cord injury: towards clinical translation of experimental strategies. Lancet Neurol. 2014; 13: 1241–1256. [Medline] [CrossRef]

34. Sangari S, Lundell H, Kirshblum S, Perez MA. Residual descending motor pathways influence spasticity after spinal cord injury. Ann Neurol. 2019; 86: 28–41. [Medline]

35. Freund P, Seif M, Weiskopf N, Friston K, Fehlings MG, Thompson AJ, et al. MRI in traumatic spinal cord injury: from clinical assessment to neuroimaging biomarkers. Lancet Neurol. 2019; 18: 1123–1135. [Medline] [CrossRef]

36. Talbott JF, Whetstone WD, Readdy WJ, Ferguson AR, Bresnahan JC, Saigal R, et al. The Brain and Spinal Injury Center score: a novel, simple, and reproducible method for assessing the severity of acute cervical spinal cord injury with axial T2-weighted MRI findings. J Neurosurg Spine. 2015; 23: 495–504. [Medline] [CrossRef]

37. Aarabi B, Sansur CA, Ibrahimi DM, Simard JM, Hersh DS, Le E, et al. Intramedullary lesion length on postoperative magnetic resonance imaging is a strong predictor of ASIA impairment scale grade conversion following decompressive surgery in cervical spinal cord injury. Neurosurgery. 2017; 80: 610–620. [Medline] [CrossRef]

38. Le E, Aarabi B, Hersh DS, Shanmuganathan K, Diaz C, Massetti J, et al. Predictors of intramedullary lesion expansion rate on MR images of patients with subaxial spinal cord injury. J Neurosurg Spine. 2015; 22: 611–621. [Medline] [CrossRef]

39. Huber E, Lachappelle P, Sutter R, Curt A, Freund P. Are midsagittal tissue bridges predictive of outcome after cervical spinal cord injury? Ann Neurol. 2017; 81: 740–748. [Medline] [CrossRef]

40. Zhang J, Jones M, DeBoy CA, Reich DS, Farrell JAD, Hoffman PN, et al. Diffusion tensor magnetic resonance imaging of Wallerian degeneration in rat spinal cord after dorsal root axotomy. J Neurosci. 2009; 29: 3160–3171. [Medline] [CrossRef]

41. Budde MD, Xie M, Cross AH, Song SK. Axial diffusivity is the primary correlate of axonal injury in the experimental autoimmune encephalomyelitis spinal cord: a quantitative pixelwise analysis. J Neurosci. 2009; 29: 2805–2813. [Medline] [CrossRef]

42. Tu TW, Kim JH, Wang J, Song SK. Full tensor diffusion imaging is not required to assess the white-matter integrity in mouse contusion spinal cord injury. J Neurotrauma. 2010; 27: 253–262. [Medline] [CrossRef]

43. Benjamini D, Hutchinson EB, Komlosh ME, Comrie CJ, Schwerin SC, Zhang G, et al. Direct and specific assessment of axonal injury and spinal cord microenvironments using diffusion correlation imaging. Neuroimage. 2020; 221: 117195. [Medline] [CrossRef]

44. Rosenzweig ES, Courtine G, Jindrich DL, Brock JH, Ferguson AR, Strand SC, et al. Extensive spontaneous plasticity of corticospinal projections after primate spinal cord injury. Nat Neurosci. 2010; 13: 1505–1510. [Medline] [CrossRef]

45. Courtine G, Song B, Roy RR, Zhong H, Herrmann JE, Ao Y, et al. Recovery of supraspinal control of stepping via indirect propriospinal relay connections after spinal cord injury. Nat Med. 2008; 14: 69–74. [Medline] [CrossRef]

46. Engel-Haber E, Zeilig G, Haber S, Worobey L, Kirshblum

S. The effect of age and injury severity on clinical prediction rules for ambulation among individuals with spinal cord injury. Spine J. 2020; 20: 1666–1675. [Medline] [CrossRef]

47. Konomi T, Suda K, Ozaki M, Harmon SM, Komatsu M, Iimoto S, et al. Predictive factors for irreversible motor paralysis following cervical spinal cord injury. Spinal Cord. 2021; 59: 554–562. [Medline] [CrossRef]

48. Scivoletto G, Tamburella F, Laurenza L, Torre M, Molinari M. Who is going to walk? A review of the factors influencing walking recovery after spinal cord injury. Front Hum Neurosci. 2014; 8: 141. [Medline] [CrossRef]

49. Belliveau T, Jette AM, Seetharama S, Axt J, Rosenblum D, Larose D, et al. Developing artificial neural network models to predict functioning one year after traumatic spinal cord injury. Arch Phys Med Rehabil. 2016; 97: 1663–1668.e3. [Medline] [CrossRef]

50. Sharif S, Jazaib Ali MY. Outcome prediction in spinal cord injury: myth or reality. World Neurosurg. 2020; 140: 574–590. [Medline] [CrossRef]

51. Kirshblum S, Snider B, Eren F, Guest J. Characterizing natural recovery after traumatic spinal cord injury. J Neurotrauma. 2021; 38: 1267–1284. [Medline] [CrossRef]

52. Pfyffer D, Vallotton K, Curt A, Freund P. Predictive value of midsagittal tissue bridges on functional recovery after spinal cord injury. Neurorehabil Neural Repair. 2021; 35: 33–43. [Medline] [CrossRef]

53. van Middendorp JJ, Hosman AJF, Donders ART, Pouw MH, Ditunno JF Jr, Curt A, et al. EM-SCI Study Group. A clinical prediction rule for ambulation outcomes after traumatic spinal cord injury: a longitudinal cohort study. Lancet. 2011; 377: 1004–1010. [Medline] [CrossRef]

54. Hicks KE, Zhao Y, Fallah N, Rivers CS, Noonan VK, Plashkes T, et al. RHSCIR Network. A simplified clinical prediction rule for prognosticating independent walking after spinal cord injury: a prospective study from a Canadian multicenter spinal cord injury registry. Spine J. 2017; 17: 1383–1392. [Medline] [CrossRef]

55. Zörner B, Blanckenhorn WU, Dietz V, Curt A. EM-SCI Study Group. Clinical algorithm for improved prediction of ambulation and patient stratification after incomplete spinal cord injury. J Neurotrauma. 2010; 27: 241–252. [Medline] [CrossRef]

56. Wichmann TO, Jensen MH, Kasch H, Rasmussen MM. Early clinical predictors of functional recovery following traumatic spinal cord injury: a population-based study of 143 patients. Acta Neurochir (Wien). 2021; 163: 2289–2296 [CrossRef]. [Medline]

57. Kaminski L, Cordemans V, Cernat E, M'Bra KI, Mac-Thiong JM. Functional outcome prediction after traumatic spinal cord injury based on acute clinical factors. J Neurotrauma. 2017; 34: 2027–2033. [Medline] [CrossRef]

58. Takeoka A, Vollenweider I, Courtine G, Arber S. Muscle spindle feedback directs locomotor recovery and circuit reorganization after spinal cord injury. Cell. 2014; 159: 1626–1639. [Medline] [CrossRef]

59. Li R, Huang ZC, Cui HY, Huang ZP, Liu JH, Zhu QA, et al. Utility of somatosensory and motor-evoked potentials in reflecting gross and fine motor functions after unilateral cervical spinal cord contusion injury. Neural Regen Res. 2021; 16: 1323–1330. [Medline] [CrossRef]

60. Yang JF, Gorassini M. Spinal and brain control of human walking: implications for retraining of walking. Neuroscientist. 2006; 12: 379–389. [Medline] [CrossRef]

61. Meyer C, Filli L, Stalder SA, Awai Easthope C, Killeen T, von Tscharner V, et al. Targeted walking in incomplete spinal cord injury: role of corticospinal control. J Neurotrauma. 2020; 37: 2302–2314. [Medline] [CrossRef]

62. Filipp ME, Travis BJ, Henry SS, Idzikowski EC, Magnuson SA, Loh MYF, et al. Differences in neuroplasticity after spinal cord injury in varying animal models and humans. Neural Regen Res. 2019; 14: 7–19. [Medline] [CrossRef]

63. Smith PM, Jeffery ND. Spinal shock--comparative aspects and clinical relevance. J Vet Intern Med. 2005; 19: 788–793. [Medline]

64. Shimada K, Tokioka T. Sequential MR studies of cervical cord injury: correlation with neurological damage and clinical outcome. Spinal Cord. 1999; 37: 410–415. [Medline] [CrossRef]

65. Zhao C, Bao SS, Xu M, Rao JS. Importance of brain alterations in spinal cord injury. Sci Prog. 2021; 104: 368504211031117. [Medline] [CrossRef]

66. Isa T. The brain is needed to cure spinal cord injury. Trends Neurosci. 2017; 40: 625–636. [Medline] [CrossRef]

67. Furlan JC, Fehlings MG. The impact of age on mortality, impairment, and disability among adults with acute traumatic spinal cord injury. J Neurotrauma. 2009; 26: 1707–1717. [Medline] [CrossRef]